Supplementary Information

Direct Interaction of Actin Filaments with F-BAR Protein Pacsin2

Julius Kostan, Ulrich Salzer, Albina Orlova, Imre Törö, Vesna Hodnik, Yosuke Senju, Juan Zou, Claudia Schreiner, Julia Steiner, Jari Meriläinen, Marko Nikki, Ismo Virtanen, Oliviero Carugo, Juri Rappsilber, Pekka Lappalainen, Veli-Pekka Lehto, Gregor Anderluh, Edward H. Egelman, Kristina Djinović-Carugo

Supplementary Figures

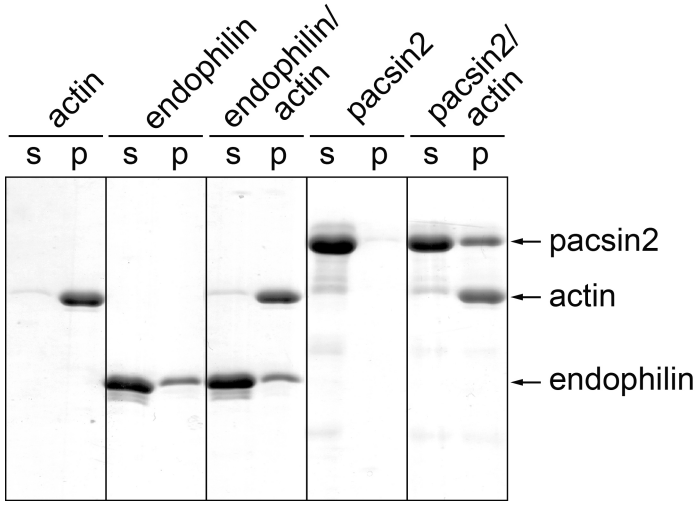

Figure S1: Pacsin2 co-sediments with actin filaments, while endophilin A1 does not.
F-actin (6 µM) was mixed with either endophilin BAR domain (endophilin) or full-length pacsin2 (both at 9 µM) in 1x F-buffer. Actin filaments and proteins bound were sedimented by centrifugation, and equal amounts of supernatant (*s*) and pellet (*p*) fractions were subjected to SDS-PAGE; separated proteins were visualized by Coomassie Brilliant Blue staining. Note: endophilin sediments in the presence of the actin to similar extent as in its absence, indicating its unspecific self-association/aggregation and not binding to the actin.

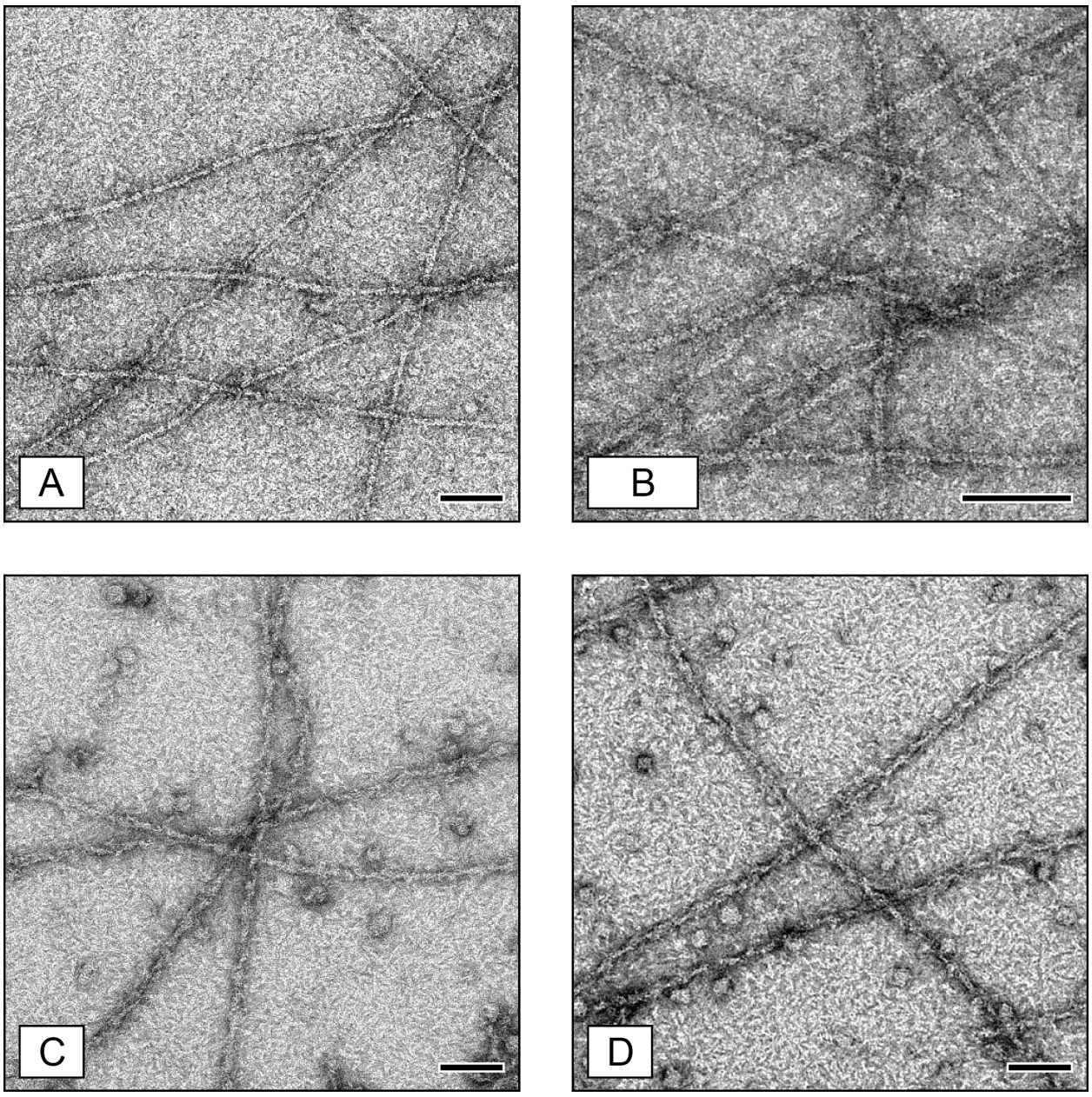

Figure S2: Pacsin2tr decorates actin filaments, while endophilin does not.
Electron micrographs of negatively stained F-actin incubated for 20 minutes either with endophilin (A, B) or with pacsin2tr for 10 min (C), or 20 min (D). The scale bar represents 100 nm.

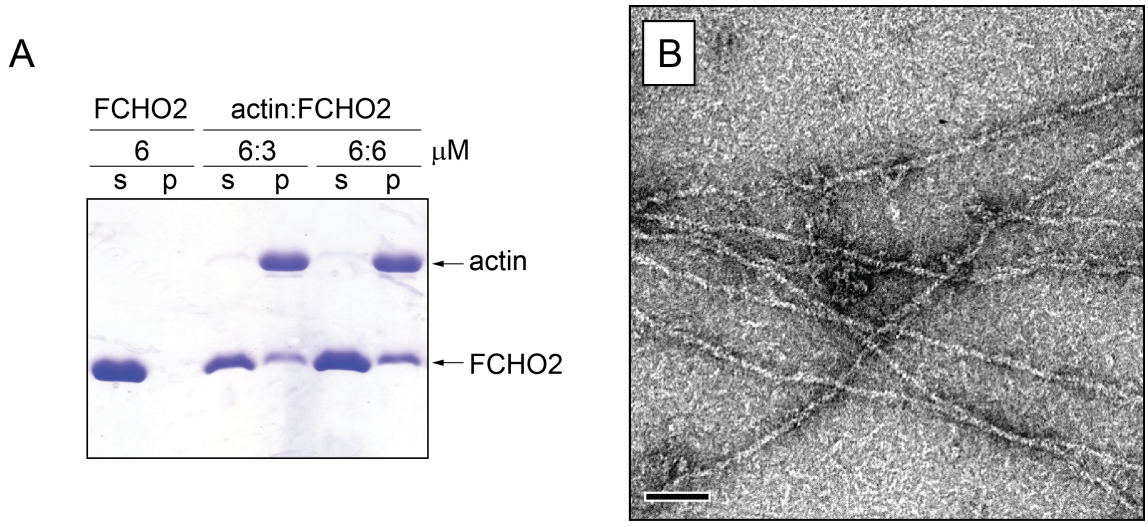

Figure S3: Unspecific association of FCHO2 with actin filaments.
(A) FCHO2 was analyzed in co-sedimentation assay after incubation with or without preassembled actin filaments at final concentration as shown on the figure. Actin filaments and proteins bound were sedimented by centrifugation, and equal amounts of supernatant (*s*) and pellet (*p*) fractions were subjected to SDS-PAGE; separated proteins were visualized by Coomassie Brilliant Blue staining. (B) Electron micrograph of negatively stained F-actin (2 μM) incubated with FCHO2 (10 μM) for 20 minutes show no association of FCHO2 with actin filaments. Thus association with F-actin, as observed in co-sedimentation assay, was not confirmed by EM, where the protein was found to form aggregates surrounding naked actin filaments. The scale bar represents 100 nm.

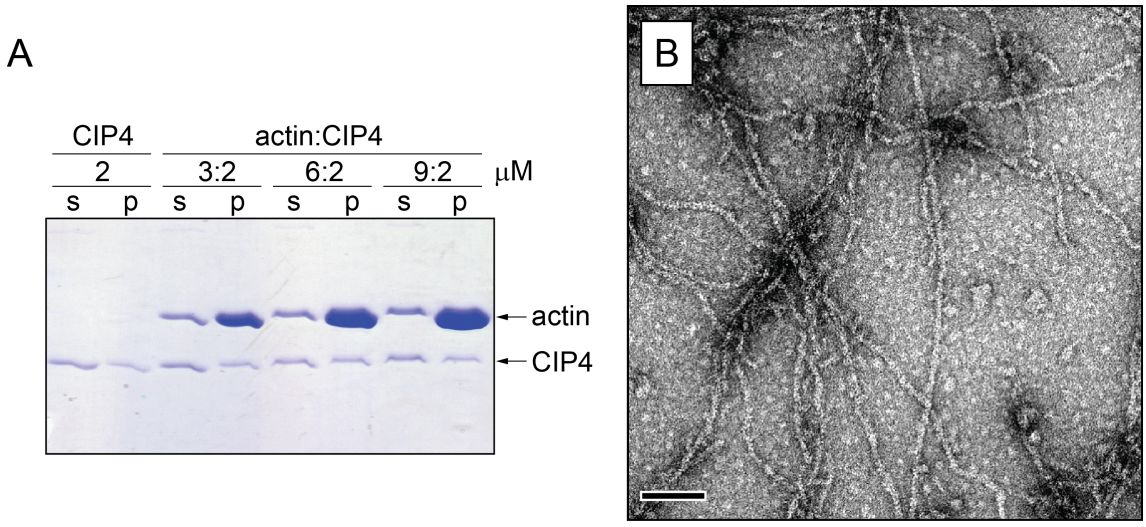

Figure S4: F-BAR domain protein CIP4 do not associate with actin filaments.
(A) CIP4 was analyzed in co-sedimentation assay after incubation with or without preassembled actin filaments at final concentration as shown on the figure. Actin filaments and proteins bound were sedimented by centrifugation, and equal amounts of supernatant (*s*) and pellet (*p*) fractions were subjected to SDS-PAGE; separated proteins were visualized by Coomassie Brilliant Blue staining. Sedimentation of CIP4 (as visible in the pellet fraction) did not depend on the presence or absence of the F-actin. (B) Electron micrograph of negatively stained F-actin (2 μM) incubated with CIP4 (app. 10 μM) for 20 minutes shows no association of CIP4 with actin filaments. The scale bar represents 100 nm.

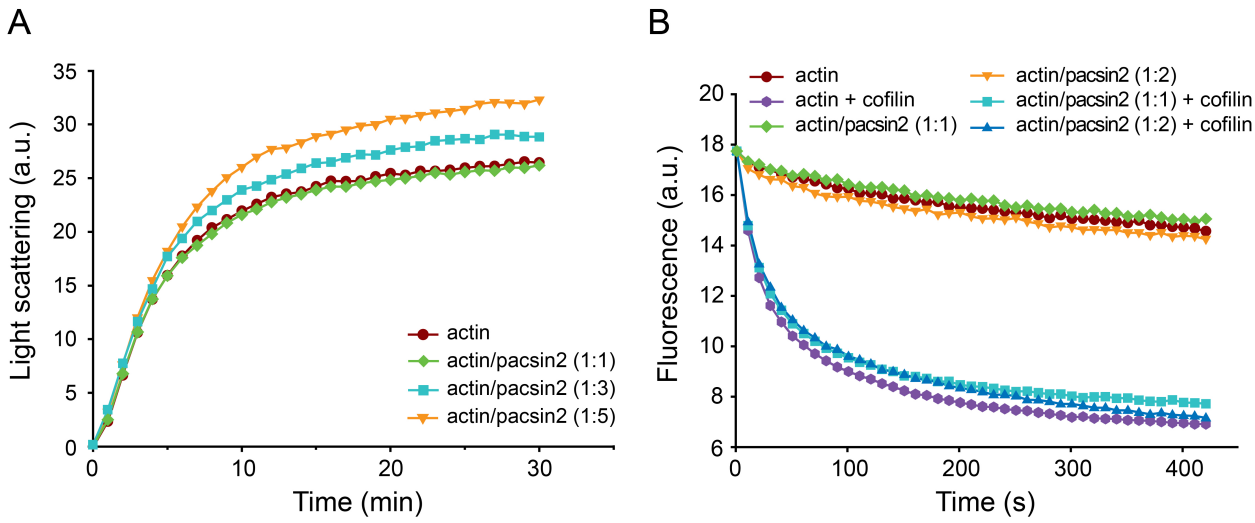

Figure S5: Effects of pacsin2 on actin dynamics.

(A) Actin filaments were polymerized at 3 µM from unlabelled rabbit muscle skeletal actin in the presence or absence of pacsin2 (at molar ratios indicated in the figure). The time course of polymerization was measured as changes in light scattering (excitation and emission set at 400 nm). (B) Effects of pacsin2 on dilution-induced actin depolymerization. Actin filaments (4 µM containing 25% pyrene-labeled actin) were pre-incubated with or without pacsin2 (at molar ratios as indicated in the figure) and diluted 20-fold (final concentration of 200 nM) to induce actin depolymerization in the presence or absence of 100 nM cofilin. The plot of fluorescence intensity of pyrene-actin against time after dilution representing the results of typical experiment is shown.

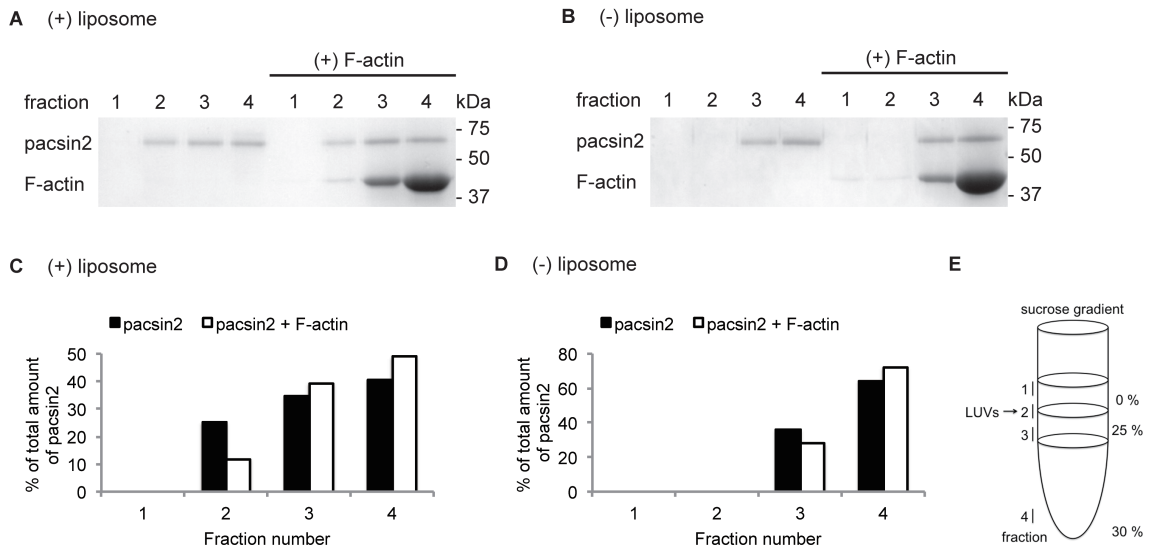

Figure S6: Membrane binding of pacsin2 in the presence and absence of F-actin examined by co-flotation assay.

(A and B) Coomassie Brilliant Blue stained gels of different fractions from co-flotation assays carried out in the presence and absence of F-actin and liposomes. (C and D) Quantification of the amount of pacsin2 in each fraction as estimated by densitometry analysis of Coomassie Brilliant Blue stained gel. (E) Schematic diagram of sucrose gradient fractions of co-flotation assay. Note: fluorescently-labeled liposomes were mostly present in fraction 2, which was detected by the intensity of Rhodamine-PE. Pacsin2, liposome and F-actin concentrations in the assay were 1 µM, 100 µM and 20 µM, respectively.

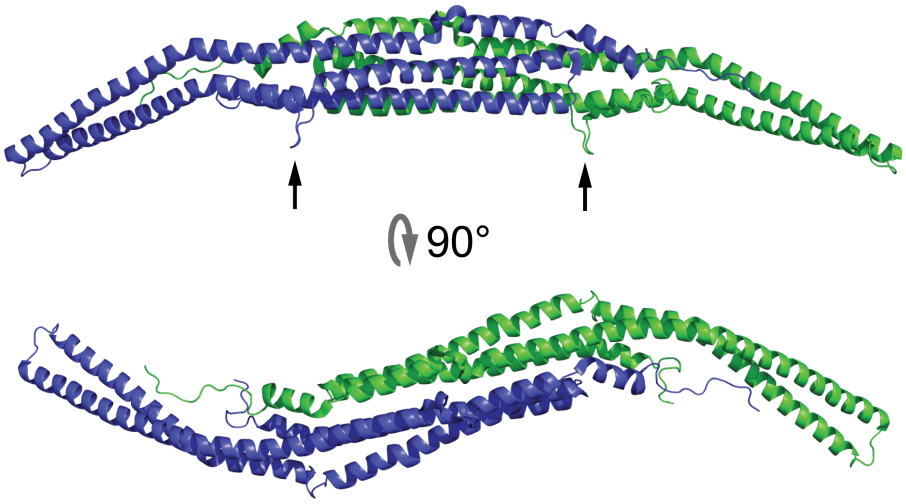

Figure S7: Structure of chicken pacsin2.

Full-length chicken pacsin2 was expressed, purified, and crystallized in two crystal forms. The phases were obtained using xenon derivatisation, as reported previously (1). The first crystal form was used to build a model encompassing residues 15-304, corresponding to the F-BAR domain. According to mass-spectrometry analysis, the peptide chain incorporated in the crystals comprises the N-terminal pGEX-2TK linker and the sequence of pacsin2 up to residue 315, suggesting a proteolytic cleavage of the C-terminal SH3 domain and the preceding linker in the course of the crystallization process. F-BAR dimer of the chicken pacsin2 is shown as cartoon. Individual subunits are colored in blue and green. Arrows indicate the unique wedge loop in the pacsin family proteins that is not found in any other F-BAR domain structure.

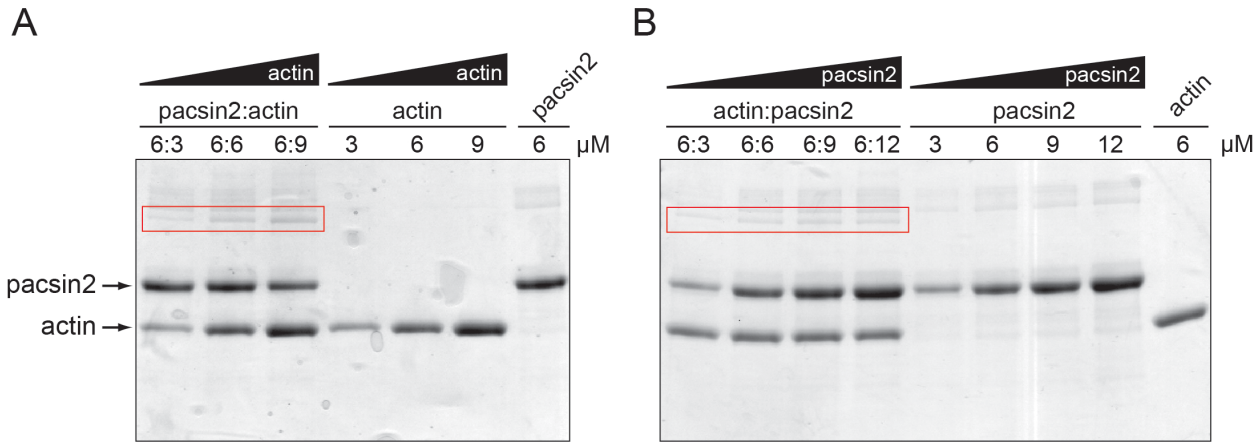

Figure S8: Cross-linking of pacsin2 with actin.

F-actin and pacsin2 were mixed at the concentration indicated on the figure and cross-linked by addition of EDC, a zero-length crosslinker, for 30 minutes at RT. SDS-PAGEs of cross-linked samples stained with Coomassie Brilliant Blue are shown. Specific band, corresponding to about 90 kDa (shown in red box/ frame) appeared after cross-linking in protein concentration dependent manner. In control experiments, where actin or pacsin2 were incubated with crosslinker alone, formation of this band has not been observed. Specific, but less abundant bands with higher molecular weight were also observed, however they were not further analyzed.

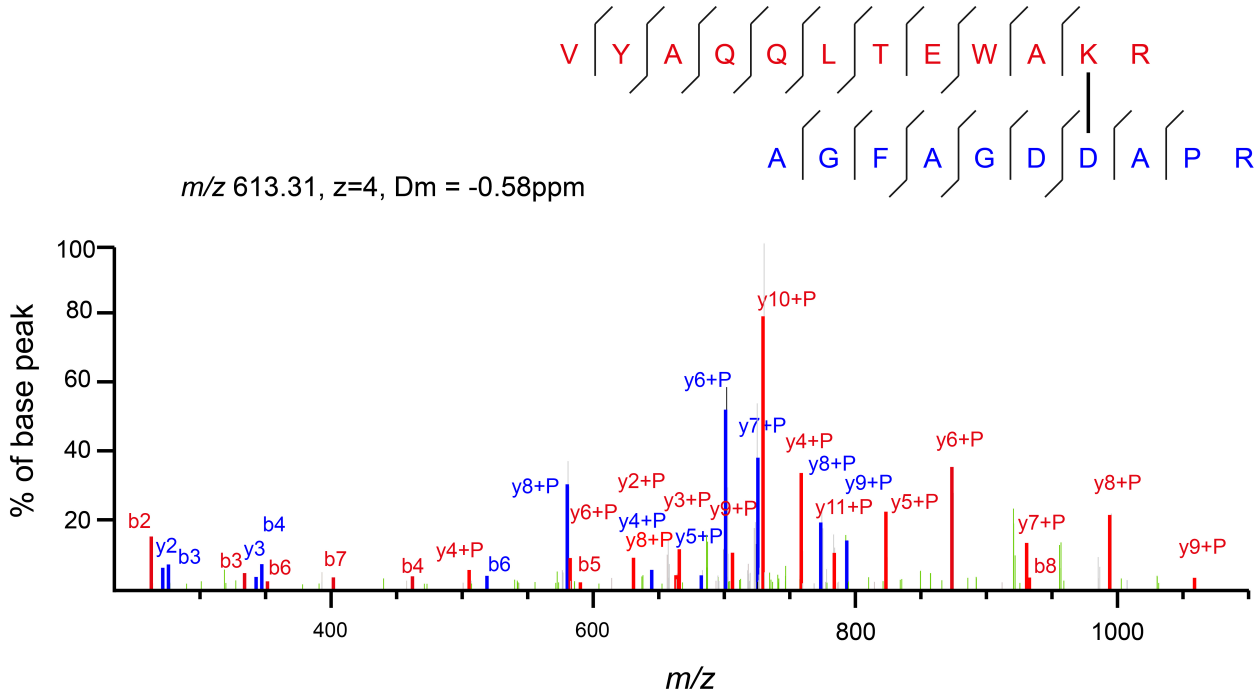

Figure S9: A representative MS/MS spectrum of a specific cross-linking product identifying a linkage between Lys64 of pacsin2 (red) and Asp25 of actin (blue).

Fragmentation spectrum of *m/z* 613.31 and the matched crosslinked peptide are shown. Only the most intense fragments are annotated in the spectrum.

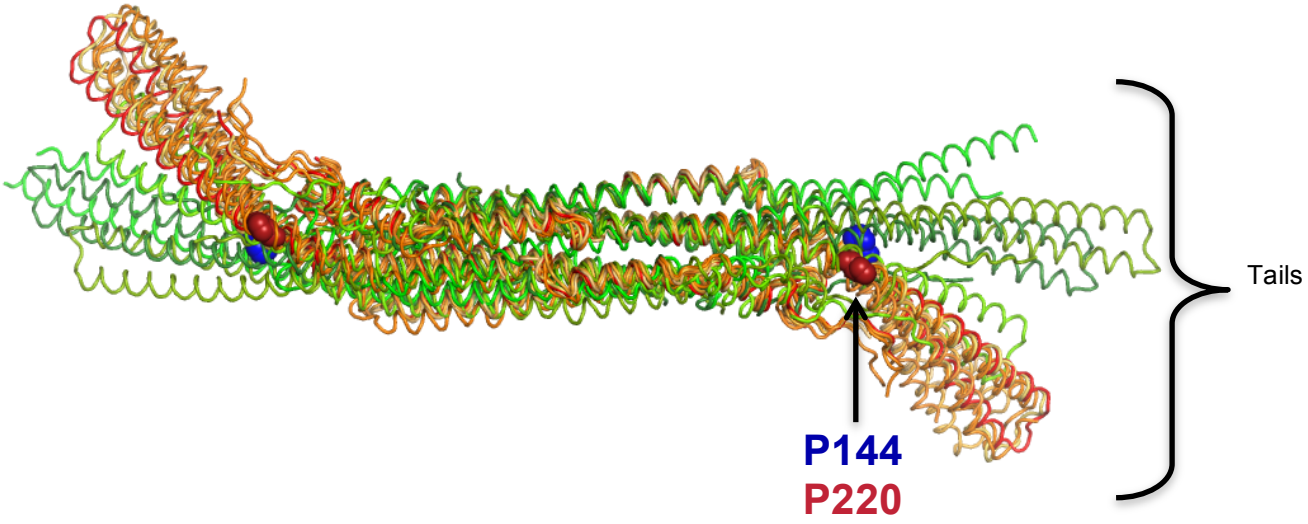

Figure S10: Structural plasticity of F-BAR domains.

Superpositions of various F-BAR-domain structures represented in ribbon. Apart from the central six-helix bundle, which is a common rigid feature of this protein family, the tails encompassing residues between 140 - 220 (pacsin2 numbering) accommodate very variable conformations. The pacsin2 type proteins (orange shades, pacsin2 is colored in red) do not deviate significantly in 3D structure and display an S-shape. The non-pacsin2 type family members lacking the apolar wedge loop (green shades) display a more straight conformation along the main axis of the six-helix bundle. Helix-breaking residues Pro144 and Pro220, generating the kink in pacsin2 are highlighted in blue and brick red, respectively. The PDB entries of the pacsins: human pacsin2 (3haj) (2), mouse pacsin2 (3lll) (3), drosophila syndapin/pacsin (3i2w) (4), human pacsin1 (3hah) (2), mouse pacsin1 (2x3v) (5), the non-pacsin F-BAR proteins: GEM interacting protein (3qwe), yeast Cdc42-interacting protein 4 (2efk) (6), human FCHO2 protein (2v0o) (7), human formin-binding protein 17 (2efl) (6).

```
PICK1             203 ASEAFVKFADAHRSIEKFGIRLLKTIK-PMLTDLNTYLNKAIPDTRLTIKKYLDVKFEYLSYCLK 266
Endophilin A1     110 FGPALGEVGEAMRELSEVKDSLDIEVKQNFIDPLQNLHDKDLREIQHHLKKLEGRRLDFDYKKKR 174
Appl1              82 MSSTLQQFSKVIDELSSCHAVLSTQLADAXXFPITQFKERDLKEILTLKEVFQIASNDHDAAINR 146
Amphiphysin2      106 ---GRDEANKIAENNDLLWMDYHQKLVDQALLTMDTYL-GQFPDIKSRIAKRGRKLVDYDSARHH 166
Arfaptin2          84 --EEFGYNAETQKLLCKNGETLLGAVNFFVSSINTLVT-KTMEDTLMTVKQYEAARLEYDAYRTD 145
Sorting Nexin 9   460 LNDAITEAGKTYEEIASLVAEQPKKDLHFLXECNHEYK-GFLGCFPDIIGTHKGAIEKVKESDKL 523
```

Figure S11: Structure-based sequence alignment of N-BAR proteins.

Structure based alignment of N-BAR proteins was taken from Conserved Domains Database (http://www.ncbi.nlm.nih.gov/Structure/cdd/cddsrv.cgi?uid=264507) (8). Selected sequences are presented here from the structures 1X03:A (endophilin A1), 2FIC:A (amphiphysin2), 1I49:A (arfaptin2), 2ELB:A (Appl1), 2RAI:A (Sorting Nexin 9) and sequence of GI:341941252 (PICK1). The position of the putative actin binding motif of PICK1 (shown in red) is boxed in green.

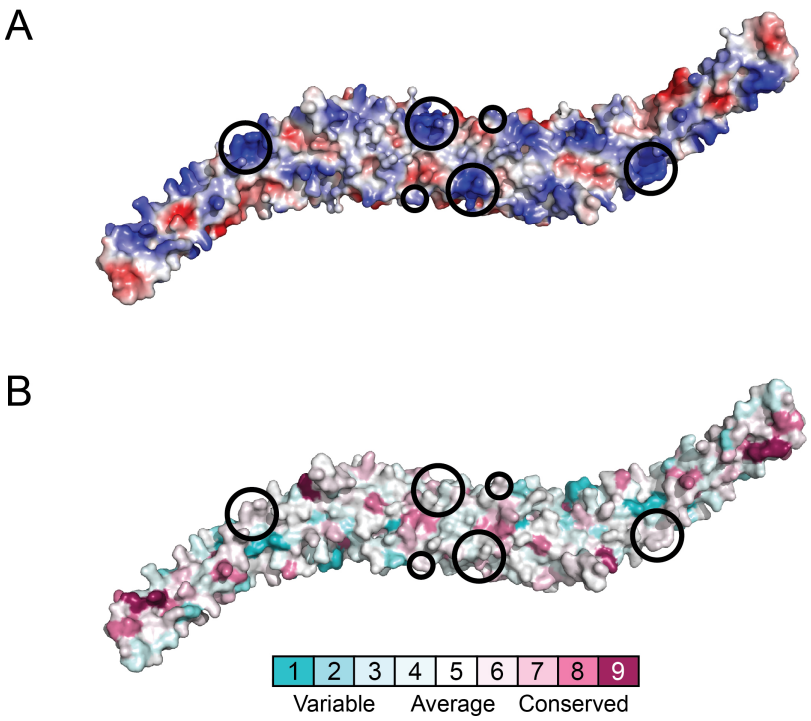

Figure S12: Conservation of the lysine clusters of pacsin2 identified by cross-linking analysis of F-actin-pacsin2 complex.

(A) Electrostatic potential of the concave surface of pacsin2. Blue and red depict positive and negative electrostatic potential, respectively; with a range of ± 7k_BT/e. Black circles highlight the positions of the lysine clusters identified by cross-linking analysis as shown in Fig 4A. (B) Conservation of residues found on the concave site of pacsin 2 as calculated by ConSurf (9) using the structure of pacsin2 (4BNE) and multiple sequence alignment built with Expresso (10). For structure based sequence alignment following sequences were used: pacsin2 (O13154), pacsin1 (Q9BY11), FCHO2 (Q0JRZ9), CIP4 (Q15642), FBP17 (Q96RU3), SYP1 (P25623), TOCA1 (Q19253), PPIP1 (P97814), GAS7 (O60861), SRGP1 (Q91Z69), FER (P16591), Nostrin (Q6WKZ7), FES (P07332), PPIP2 (Q9H939), SRGP2 (O75044). Black circles as in A.

Supplementary Table S1

Data collection and refinement statistics

DATA COLLECTION	
Source	ESRF ID-14-1
Wavelength (Å)	0.934
Resolution (Å)	53.45-2.57 (2.66-2.57)[a]
Space group	$P2_12_12_1$
Unit cell (Å)	a = 101.06, b = 105.50, c = 125.95
Molecules / a.u.	2
Total reflections	195103 (11479)
Unique reflections	41812 (3322)
Completeness (%)	95.99 (77.47)
R_{merge}[b]	0.077 (0.682)
R_{meas}[c]	0.087 (0.792)
R_{pim}[d]	0.039 (0.394)
Multiplicity	4.66 (3.46)
<I/σ(I)>	15.1 (2.2)
Wilson B-factor	49.93
REFINEMENT	
Number of (non hydrogen) atoms	5056
Macromolecules	4816
Ligands	55
Water	185
Protein residues	579
R_{cryst}[e] / R_{free}[f]	0.1838 (0.2854)/0.2222 (0.3190)
R.m.s.d. bonds (Å)	0.002
R.m.s.d. angles (º)	0.52
Ramachandran favored (%)	98
Ramachandran outliers (%)	0
Molprobity clashscore	1.56
Average B-fator (Ă^2)	64.6
Macromolecules	64.7
Ligands	83.7
Solvent	55.7

[a] Values in parentheses are for the highest resolution shell.

[b] R_{merge} (R_{sym}) = Σ | Ihl - <Ih> | / Σ | <Ih> |

[c] $$R_{meas} = \frac{\sum_h \sqrt{\frac{n_h}{n_h - 1}} \sum_i^{n_h} \left| \hat{\mathrm{I}}_h - \mathrm{I}_{h,i} \right|}{\sum_h \sum_i^{n_h} \mathrm{I}_{h,i}} \text{ with } \hat{I}_h = \frac{1}{n_h} \sum_i^{n_h} \mathrm{I}_{h,i}$$

[d] $$R_{pim} = \sum_{\mathrm{hkl}} \sqrt{\frac{1}{N-1}} \sum_i \left| \mathrm{I}_{\mathrm{i}}(hkl) - \overline{\mathrm{I}(\mathrm{hkl})} \right| / \sum_{\mathrm{hkl}} \sum_{\mathrm{i}} \mathrm{I}_{\mathrm{i}}(hkl)$$

Where I (hkl) is the mean intensity of multiple I_i (*hkl*) observations of the symmetry-related reflections, N is the redundancy, n_h is the multiplicity, $\hat{I}_h$ is the average intensity and $I_{h,i}$ is the observed intensity.

[e] R_{cryst} = Σ | F_o-F_c| / Σ F_o

[f] R_{free} is the cross-validation R_{factor} computed for the test set of reflections (5 %) which are omitted in the refinement process.

Supplementary Table S2

Cross-link sites identified for complex of pacsin2 with F-actin.
Residues clustering close on the protein surface (as shown on the Fig 4A and B) are highlighted with the same colour.

From Protein	From Residue	To Protein	To Residue	Score	Cα-Cα distance (Å)
pacsin2	**K 64**	actin	**D 25**	12.502	13.6
pacsin2	**K 64**	actin	**E 100**	11.724	18.7
pacsin2	**K 101**	actin	**D 25**	11.397	13.4
pacsin2	**K 53**	actin	**E 100**	9.143	12.5
pacsin2	**K 143**	actin	**E 100**	9.083	16.5
pacsin2	**K 150**	actin	**D 25**	8.960	11.5
pacsin2	**K 101**	actin	**D 24**	8.081	19.5
pacsin2	**K 53**	actin	**E 99**	7.870	15.6
pacsin2	**K 147**	actin	**D 24**	7.110	10.8
		Internal peptides			
pacsin2	**K67**	pacsin2	**E424**	9.372	
pacsin2	**K146**	pacsin2	**E406**	7.642	

Supplementary Methods

Plasmids and DNA Constructs

Cloning, expression and purification of N-terminal GST-fused pacsin2 used for crystallization and structure determination was described elsewhere (1). For the bacterial expression of proteins with N-terminal His, or Strep II tags, PCR products of the cDNA encoding the full-length pacsin2 (residues 1-448; numbering of amino acids follows sequence of pacsin2 described in Meriläinen et al. (11), its truncated variant pacsin2tr (residues 1-324), rat endophilin A1 N-BAR domain (residues 1-247), F-BAR domain of human CIP4 (residues 10-303), and F-BAR domain of human FCHO2 (residues 3–274) were subcloned into pETM14 (EMBL) and modified pET21b vector (Merck) encoding N-terminal Strep II followed with TEV cleavage site before starting codon. To obtain plasmids for expression of the mutant variants of both pacsin2 and pacsin2tr, where either alanine was substituted for residue Met124 (pacsin2-M124A, and pacsin2tr-M124A), or glycine for loop encoded by His121-Met125 (pacsin2-Δ1, and pacsin2tr-Δ1), or Met124 and Met125 were deleted (pacsin2-Δ2, and pacsin2tr-Δ2), mutagenesis was carried out using the QuickChange site-directed mutagenesis kit (Stratagene). The plasmids encoding the N-terminal Strep II-tag fusion wild-type or C-terminally truncated variant of pacsin2 (pacsin2tr) were used as template. All of the constructs were verified by DNA sequence analysis. Preparation/cloning of expression plasmid encoding N-terminally GST-tagged version of full-length mouse cofilin-1 (pPL92) was described previously (Vartiainen et al., 2002).

Protein Expression and Purification

All of the recombinant pacsin2 variants as well as endophilin A1 N-BAR domain, and F-BAR domains of CIP4 and FCHO2 were overexpressed in the *E. coli* strain Rosetta 2 (Merck). Proteins were expressed at 18 °C, either in LB medium after induction with 0.4 mM isopropyl β-d-thiogalactopyranoside (IPTG) at an A600 of 0.6, or in ZY5052 auto-induction media (Studier, 2005) for 12-18 hours. The N-terminal His- and Strep II-tagged fusion proteins were purified by affinity chromatography using HisTrap HP, and StrepTrap HP columns (GE Healthcare), respectively. When needed, the His-tag or Strep II-tag were cleaved overnight (at 4°C) with TEV or 3C/PreScission Protease. Proteins were further purified by size exclusion chromatography on a HiLoad 26/60 Superdex 200 Prep Grade column (GE Healthcare) equilibrated with 20 mM Hepes, 150 mM NaCl, pH 7.5, or 8.0 with or without addition of 5 % glycerol. For endophilin A1 N-BAR domain, solution containing 20 mM Hepes, 250 mM NaCl, pH 8.0 was used to equilibrate the column. Protein purity and monodispersity was judged by SDS-PAGE and dynamic light

scattering, respectively. Mouse cofilin was expressed and purified as described in Vartiainen et al. (12). Actin was prepared from rabbit skeletal muscle (13) and pyrene labeled following Kouyama and Mihashi (14).

F-Actin Polymerisation Assays

Before the experiments, Ca^{2+}-ATP–actin was converted into Mg^{2+}-ATP–actin by addition of 10x magnesium-exchange buffer (0.5 mM $MgCl_2$, 20 mM EGTA, pH 7.4) and used 3 min later. For assembly assays, dilutions of proteins to be assayed (as described in the figure legends) were prepared in 1x KMEI buffer (50 mM KCl, 1 mM $MgCl_2$, 1 mM EGTA, 5 mM imidazole, pH 7.0). The assembly reaction was initiated by transferring 117 µl of the protein solution to 13 µl of 30 µM solution of G-actin in G-buffer. The polymerization of actin was followed by measuring the light-scattering at 22°C, for at least 35 min in a Jasco FP-6300 fluorescence spectrophotometer with excitation and emission set at 400 nm. Alternatively, actin polymerization rates were followed as increase in the pyrene fluorescence (excitation 365 nm, emission 388 nm) at room temperature using a 10% pyrene-labeled actin in 1x KMEI buffer.

F-Actin Depolymerisation Assays

Pyrene-labeled-F-actin filaments (4 µM or 1.8 µM, 25% pyrene labelled) were prepared by a 1 hour incubation at room temperature in 1x F-buffer in the presence or absence of different concentration of pacsin2 as described in the figure legends. Depolymerization of actin filaments was induced by 20x dilution with 1x F-buffer to a final concentration of 0.2 µM in the presence or absence of cofilin at the concentration indicated in the legends of the figures. Pre-cut pipet tips were used for all manipulations of actin filaments, and care was taken to avoid filament shearing. Pyrene fluorescence was monitored at room temperature over time at an excitation of 365 nm and emission of 388 nm in a Jasco FP-6300 fluorescence spectrophotometer.

Cross-Linking and Mass Spectrometry Analyses

For cross-linking experiments, actin and pacsin2 were mixed at the concentration as indicated on the figure (**Supplementary Fig S8**) in 40 μl of 10 mM PIPES, 50 mM KCl, 2 mM $MgCl_2$, pH 6.8, and incubated for 30 minutes at room temperature. Afterwards, a zero-length cross-linking agent, 1-ethyl-3-[3-dimethylaminopropyl] carbodiimide hydrochloride (EDC, Thermo Fisher Scientific) was added to final concentration of 1 mM and proteins were cross-linked for additional 30 minutes. The reaction was

stopped by adding 5x Laemmli sample buffer. Samples were separated by SDS-PAGE and stained with Coomassie Blue G-250. The band corresponding to cross-linked complexes was excised, and the proteins therein were reduced using 10 mM DTT for 30 min at 37°C, alkylated with 55 mM iodoacetamide for 20 min in the dark at room temperature, and digested using 13 ng/µL trypsin (sequencing grade; Promega) overnight at 37°C (15).

The digested peptides were desalted using C18-Stage-Tips (16), and analysed on LTQ Orbitrap Velos (Thermo Fisher Scientific) coupled with Dinex Ultimate 3000 RSLC nano system. The column with a spray emitter (75-µm inner diameter, 8-µm opening, 250-mm length; New Objectives) that was packed with C18 material (ReproSil-Pur C18-AQ 3 µm; Dr Maisch GmbH, Ammerbuch-Entringen, Germany) using an air pressure pump (Proxeon Biosystems) (17). Mobile phase A consisted of water and 0.1% formic acid. Mobile phase B consisted of 80% ACN acetonitrile and 0.1% formic acid. Peptides were loaded onto the column with 2% B at 500 nl/min flow rate and eluted at 300 nl/min flow rate with two gradients: linear increase from 2% B to 40% B in 150 mintutes; then increase from 40% to 95% B in 11 minutes. The eluted peptides were directly sprayed into the mass spectrometer.

Peptides were analysed using a high/high strategy: both MS spectra and MS2 spectra were acquired in the Orbitrap. FTMS spectra were recorded at 100,000 resolution. The eight highest intensity peaks with a charge state of three or higher were selected in each cycle for ion trap fragmentation. The fragments were produced using CID with 35% normalized collision energy and detected by the Orbitrap at 7500 resolution. Dynamic exclusion was set to 90s and repeat count was 1 (18).

The mass spectrometric raw files were processed into peak lists using MaxQuant (version 1.3.0.5) (19) at default parameters except for “top MS/MS peaks per 100 Da” being set to 100. Search was conducted against F-actin-pacsin2 complex (is this a right description?) sequences using in-house Xi software (version 1.3.355). Search parameters were MS accuracy, 6ppm; MS/MS accuracy, 20ppm; enzyme, trypsin; cross-linker, BS3 (including BS3 modification); Max missed cleavages, 4; fixed modification, carbamidomethylation on cysteine; variable modifications, oxidation on methionine; cross-linkable amino acids, N-terminus, lysine, serine, tyrosine and threonine; fragments, b and y ions with loss of H_2O, NH_3 and CH_3SOH.

Co-floatation Assay

Large unilamellar vesicles (LUVs) with molar lipid composition of POPC:POPE:POPS:PI(4,5)P2:Rhodamine PE = 50:15:20:10:5 (Avanti Polar Lipids) were prepared as previously described (20). Purified full-length pacsin2 was incubated at the concentration of 1 µM with 100 µM LUVs in the presence and absence of

20 µM F-actin for 1 hour. The samples were centrifuged at 54 000 rpm with Beckman Optima using TLS-55 rotor (Beckman) for 30 min at 4°C. Each fraction was collected from top to bottom and equal amount of samples was run on SDS-PAGE followed by Coomassie staining. The protein amount of each band was quantified by densitometry analysis using ImageJ. The fluorescence intensity of the same fractions was measured at the wavelength of 583 nm using a LS 55 Fluorescence Spectrometer (Perkin-Elmer) to detect Rhodmaine-PE-labeled liposome fraction.

Crystallization, Data Collection and Structure Solution

Details on crystallisation, data collection and phasing are reported in Toro at al. (1). Native data was processed in XIA2 (21) using XDS (22) as the integration software.

Crystal Structure Refinement and Analysis

Electron density maps of the best phases calculated by SHARP were subjected to solvent flattening by SOLOMON (23) followed by an auto-building procedure by ARP/wARP (24) and successively in Buccaneer (25). The model was completed by manual building using COOT (26). The positional, isotropic atomic displacement parameters (ADP) and TLS (Translation/Libration/Screw) refinement was carried out by phenix.refine of the PHENIX suite (27). For TLS refinement the TLS groups were automatically determined by the software after several cycles of isotropic ADP refinement. The final refinement statistics gave excellent values for R_{work}= 0.184 and R_{free}= 0.222, as well as rmsd bond and angle values for diffraction data to 2.57 Å resolution. Data collection and refinement statistics are reported in **Supplementary Table S1**.

The geometry of the refined structure was analyzed by phenix.refine during the refinement procedure then the final model quality was assessed by molprobity (28). The water network and other bound ions were verified in COOT (26). The structural superpositions were done by SUPERIMPOSE (29). The dimer interfaces were analyzed with PISA (30). Electrostatic potentials were calculated by APBS (31), all visualizations were done in PYMOL (32).

Supplementary References

1. Toro I, Nikki M, Glumoff T, Lehto V-P, Djinovic Carugo K. Crystallization and phasing of focal adhesion protein 52 from Gallus gallus. Acta Crystallographica Section D. 2004;60(3):539-41.

2. Wang Q, Navarro MV, Peng G, Molinelli E, Goh SL, Judson BL, et al. Molecular mechanism of membrane constriction and tubulation mediated by the F-BAR protein Pacsin/Syndapin. Proceedings of the National Academy of Sciences of the United States of America. 2009;106(31):12700-5.

3. Plomann M, Wittmann JG, Rudolph MG. A hinge in the distal end of the PACSIN 2 F-BAR domain may contribute to membrane-curvature sensing. Journal of molecular biology. 2010;400(2):129-36.

4. Edeling MA, Sanker S, Shima T, Umasankar PK, Honing S, Kim HY, et al. Structural requirements for PACSIN/Syndapin operation during zebrafish embryonic notochord development. PloS one. 2009;4(12):e8150.

5. Rao Y, Ma Q, Vahedi-Faridi A, Sundborger A, Pechstein A, Puchkov D, et al. Molecular basis for SH3 domain regulation of F-BAR-mediated membrane deformation. Proceedings of the National Academy of Sciences of the United States of America. 2010;107(18):8213-8.

6. Shimada A, Niwa H, Tsujita K, Suetsugu S, Nitta K, Hanawa-Suetsugu K, et al. Curved EFC/F-BAR-domain dimers are joined end to end into a filament for membrane invagination in endocytosis. Cell. 2007;129(4):761-72.

7. Henne WM, Kent HM, Ford MG, Hegde BG, Daumke O, Butler PJ, et al. Structure and analysis of FCHo2 F-BAR domain: a dimerizing and membrane recruitment module that effects membrane curvature. Structure. 2007;15(7):839-52.

8. Marchler-Bauer A, Zheng C, Chitsaz F, Derbyshire MK, Geer LY, Geer RC, et al. CDD: conserved domains and protein three-dimensional structure. Nucleic acids research. 2013;41(Database issue):D348-52.

9. Celniker G, Nimrod G, Ashkenazy H, Glaser F, Martz E, Mayrose I, et al. ConSurf: Using Evolutionary Data to Raise Testable Hypotheses about Protein Function. Isr J Chem. 2013;53(3-4):199-206.

10. Armougom F, Moretti S, Poirot O, Audic S, Dumas P, Schaeli B, et al. Expresso: automatic incorporation of structural information in multiple sequence alignments using 3D-Coffee. Nucleic acids research. 2006;34(Web Server issue):W604-8.

11. Merilainen J, Lehto V-P, Wasenius V-M. FAP52, a Novel, SH3 Domain-containing Focal Adhesion Protein. J Biol Chem1997.

12. Vartiainen MK, Mustonen T, Mattila PK, Ojala PJ, Thesleff I, Partanen J, et al. The three mouse actin-depolymerizing factor/cofilins evolved to fulfill cell-type-specific requirements for actin dynamics. Molecular biology of the cell. 2002;13(1):183-94.

13. Spudich JA, Watt S. The regulation of rabbit skeletal muscle contraction. I. Biochemical studies of the interaction of the tropomyosin-troponin complex with actin and the proteolytic fragments of myosin. The Journal of biological chemistry. 1971;246(15):4866-71.

14. Kouyama T, Mihashi K. Fluorimetry study of N-(1-pyrenyl)iodoacetamide-labelled F-actin. Local structural change of actin protomer both on polymerization and on binding of heavy meromyosin. European journal of biochemistry / FEBS. 1981;114(1):33-8.

15. Maiolica A, Cittaro D, Borsotti D, Sennels L, Ciferri C, Tarricone C, et al. Structural analysis of multiprotein complexes by cross-linking, mass spectrometry, and database searching. Molecular & cellular proteomics : MCP. 2007;6(12):2200-11.

16. Rappsilber J, Ishihama Y, Mann M. Stop and go extraction tips for matrix-assisted laser desorption/ionization, nanoelectrospray, and LC/MS sample pretreatment in proteomics. Analytical chemistry. 2003;75(3):663-70.

17. Ishihama Y, Rappsilber J, Andersen JS, Mann M. Microcolumns with self-assembled particle frits for proteomics. Journal of chromatography A. 2002;979(1-2):233-9.

18. Abad MA, Medina B, Santamaria A, Zou J, Plasberg-Hill C, Madhumalar A, et al. Structural basis for microtubule recognition by the human kinetochore Ska complex. Nature communications. 2014;5:2964.

19. Cox J, Mann M. MaxQuant enables high peptide identification rates, individualized p.p.b.-range mass accuracies and proteome-wide protein quantification. Nature biotechnology. 2008;26(12):1367-72.

20. Pykalainen A, Boczkowska M, Zhao H, Saarikangas J, Rebowski G, Jansen M, et al. Pinkbar is an epithelial-specific BAR domain protein that generates planar membrane structures. Nature structural & molecular biology. 2011;18(8):902-7.

21. Winter G. xia2: an expert system for macromolecular crystallography data reduction. J Appl Crystallogr. 2010;43:186-90.

22. Kabsch W. Xds. Acta crystallographica Section D, Biological crystallography. 2010;66(Pt 2):125-32.

23. Abrahams JP, Leslie AGW. Methods used in the structure determination of bovine mitochondrial F1 ATPase. Acta Crystallographica Section D. 1996;52(1):30-42.

24. Lamzin VS, Wilson KS. Automated refinement of protein models. Acta Crystallographica Section D. 1993;49(1):129-47.

25. Cowtan K. Fitting molecular fragments into electron density. Acta Crystallogr D. 2008;64:83-9.

26. Emsley P, Cowtan K. Coot: model-building tools for molecular graphics. Acta Crystallographica Section D. 2004;60(12 Part 1):2126-32.

27. Adams PD, Afonine PV, Bunkoczi G, Chen VB, Davis IW, Echols N, et al. PHENIX: a comprehensive Python-based system for macromolecular structure solution. Acta Crystallogr D. 2010;66:213-21.

28. Chen VB, Arendall WB, Headd JJ, Keedy DA, Immormino RM, Kapral GJ, et al. MolProbity: all-atom structure validation for macromolecular crystallography. Acta Crystallogr D. 2010;66:12-21.

29. Diederichs K. Structural superposition of proteins with unknown alignment and detection of topological similarity using a six-dimensional search algorithm. Proteins. 1995;23(2):187-95.

30. Krissinel E, Henrick K. Inference of macromolecular assemblies from crystalline state. Journal of molecular biology. 2007;372(3):774-97.

31. Baker NA, Sept D, Joseph S, Holst MJ, McCammon JA. Electrostatics of nanosystems: Application to microtubules and the ribosome. PNAS. 2001;98(18):10037-41.

32. DeLano WL. The PyMOL Molecular Graphics System 2002.